Redox Biology 65 (2023) 102825

Contents lists available at ScienceDirect

Redox Biology

journal homepage: www.elsevier.com/locate/redox

EP1 activation inhibits doxorubicin-cardiomyocyte ferroptosis via Nrf2

Bei Wang [a,1], Yuxuan Jin [b,1], Jiao Liu [a,1], Qian Liu [a], Yujun Shen [a], Shengkai Zuo [a,c,**], Ying Yu [a,*]

[a] Department of Pharmacology, Tianjin Key Laboratory of Inflammatory Biology, Center for Cardiovascular Diseases, Key Laboratory of Immune Microenvironment and Disease (Ministry of Education), The Province and Ministry Co-sponsored Collaborative Innovation Center for Medical Epigenetics, School of Basic Medical Sciences, Tianjin Medical University, Tianjin, China

[b] Department of Cardiology, First Affiliated Hospital of Zhengzhou University, Zhengzhou, China

[c] Department of Biopharmaceutics, School of Pharmacy, Tianjin Medical University, Tianjin, China

ARTICLE INFO

Keywords:
Cardiomyocyte ferroptosis
DOX-induced cardiomyopathy
EP1
Nrf2

ABSTRACT

Chemotherapeutic agents, such as doxorubicin (DOX), may cause cardiomyopathy, even life-threatening arrhythmias in cancer patients. Ferroptosis-an iron-dependent oxidative form of programmed necrosis, plays a pivotal role in DOX-induced cardiomyopathy (DIC). Prostaglandins (PGs) are bioactive signaling molecules that profoundly modulate cardiac performance in both physiologic and pathologic conditions. Here, we found that PGE_2 production and its E-prostanoid 1 receptor (EP1) expression were upregulated in erastin (a ferroptosis inducer) or DOX-treated cardiomyocytes. EP1 inhibition markedly aggravated erastin or DOX-induced cardiomyocyte ferroptosis, whereas EP1 activation exerted opposite effect. Genetic depletion of EP1 in cardiomyocytes worsens DOX-induced cardiac injury in mice, which was efficiently rescued by the ferroptosis inhibitor Ferrostatin-1 (Fer-1). Mechanistically, EP1 activation protected cardiomyocytes from DOX-induced ferroptosis by promoting nuclear factor erythroid 2-related factor 2 (Nrf2)-driven anti-oxidative gene expression, such as glutathione peroxidase 4 (GPX4) and solute carrier family 7 member 11 (SLC7A11). EP1 was coupled with $G_{\alpha q}$ to elicit intracellular Ca^{2+} flux and activate the PKC/Nrf2 cascade in ferroptotic cardiomyocytes. EP1 activation also prevents DOX-induced ferroptosis in human cardiomyocytes. Thus, PGE_2/EP1 axis protects cardiomyocytes from DOX-induced ferroptosis by activating PKC/Nrf2 signaling and activation of EP1 may represent an attractive strategy for DIC prevention and treatment.

1. Introduction

Adverse cardiovascular events are major side effects of cancer treatment [1]. Several cardiotoxic outcomes in patients receiving oncologic treatment are asymptomatic left ventricular (LV) dysfunction, cardiomyopathy, and progressive heart failure (HF), which are reportedly responsible for approximately 60% of cardiovascular mortality in cancer patients [2]. Doxorubicin (DOX) is a very effective anti-cancer agent; however, its efficacy is limited by its persistent and cumulative cardiomyopathy [3]. The major causes of DOX-induced cardiomyopathy (DIC) are excessive reactive oxygen species (ROS) production and Top2β poisoning, which creates double-strand breaks and mitochondrial damage [4–6]. To date, dexrazoxane, an iron chelator that binds free iron and reduces oxidative stress, is the only cardiac protective drug approved by the US Food and Drug Administration for reducing the undesired side effects of DOX in advanced breast cancer [7,8]. Despite its efficacy in reducing the cardiotoxic effects of anthracyclines, dexrazoxane increases the risk of developing secondary malignant neoplasms and its use in pediatric patients is banned [9,10]. Thus, understanding the biological mechanisms underlying DOX cardiotoxicity is crucial for the development of new agents to overcome the limitations of conventional chemotherapy.

* Corresponding author. Department of Pharmacology, Tianjin Key Laboratory of Inflammatory Biology, Center for Cardiovascular Diseases, Key Laboratory of Immune Microenvironment and Disease (Ministry of Education), The Province and Ministry Co-sponsored Collaborative Innovation Center for Medical Epigenetics, School of Basic Medical Sciences, Tianjin Medical University, Tianjin, China.

** Corresponding author. Department of Pharmacology, Tianjin Key Laboratory of Inflammatory Biology, Center for Cardiovascular Diseases, Key Laboratory of Immune Microenvironment and Disease (Ministry of Education), The Province and Ministry Co-sponsored Collaborative Innovation Center for Medical Epigenetics, School of Basic Medical Sciences, Tianjin Medical University, Tianjin, China.

E-mail addresses: zuoshengkai@tmu.edu.cn (S. Zuo), yuying@tmu.edu.cn (Y. Yu).

[1] These authors contributed equally.

https://doi.org/10.1016/j.redox.2023.102825
Received 2 June 2023; Received in revised form 17 July 2023; Accepted 23 July 2023
Available online 24 July 2023

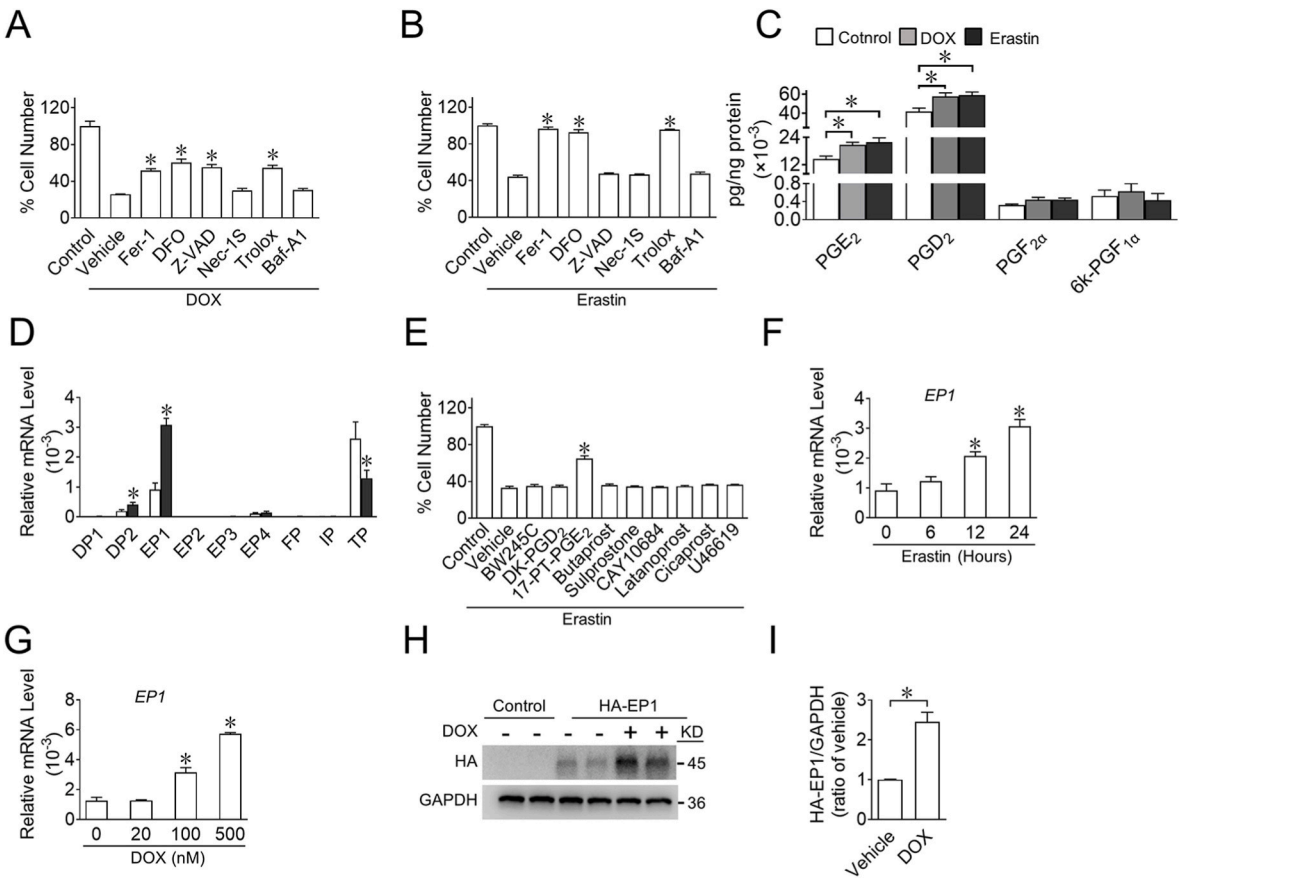

Fig. 1. EP1 expression is upregulated in cardiomyocyte in response to erastin or DOX treatment

A, B. Effect of Fer-1 (2 μM, ferroptosis inhibitor), DFO (100 μM, iron chelator), Z-VAD (10 μM, apoptosis inhibitor), Nec-1S (10 μM, necroptosis inhibitor), Trolox (100 μM, antioxidant) or Baf-A1 (1 nM, autophagy inhibitor) on living H9C2 cells treated with DOX (2 μM) (A) or erastin (3 μM) (B). *$P < 0.05$ vs vehicle; A, n = 5; B, n = 8.

C. The PG profiles of H9C2 cells challenged by erastin or DOX. H9C2 cells were treated with erastin or DOX; and arachidonic acid (30 μM) was added into culture after washing for additional 30 min, culture supernatants were collected for PG measurement. *$P < 0.05$ vs control; n = 6.

D. Relative mRNA levels of various prostaglandin receptors in H9C2 cells in response to erastin. *$P < 0.05$ vs control; n = 6.

E. Effect of various prostaglandin receptors agonist (BW245C (10 μM), DP1 agonist; DK-PGD_2 (1 μM), DP2 agonist; 17-PT-PGE_2 (2.5 μM), EP1 agonist; Butaprost (5 μM), EP2 agonist; Sulprostone (1 μM), EP3 agonist; CAY10684 (1 μM), EP4 agonist; Latanoprost (2 μM), FP agonist; Cicaprost (1 μM), IP agonist; U46619 (1 μM), TP agonist) on living H9C2 cells treated with erastin. *$P < 0.05$ vs vehicle; n = 8.

F. Time-dependent EP1 expression in H9C2 cells in response to erastin. *$P < 0.05$ vs 0 h; n = 6.

G. Dose-dependent EP1 expression in H9C2 cells in response to DOX. *$P < 0.05$ vs 0 nM; n = 4.

H. Western blot analysis of HA-EP1 expression in heart tissue from EP1-N-HA mice treated with DOX.

I. Quantification of the HA-EP1 expression in H. *$P < 0.05$ vs vehicle; n = 4.

Ferroptosis, characterized by iron-dependent ROS accumulation, is a new form of regulated cell death that differs from apoptosis, necrosis, and autophagy. Heart biopsy specimens from patients with heart failure due to DIC show iron overload in the mitochondria [5]. DOX affects iron homeostasis by inactivating iron regulatory proteins [11], reducing ferritin [12] and upregulating transferrin receptor [13]. Treatment with ferrostatin-1 (Fer-1), a ferroptosis inhibitor, improves the survival of mice with DOX. Ferroptosis is ultimately identified as the primary cause of cell death in DIC [14]. Nuclear factor erythroid 2-related factor 2 (Nrf2) is a master transcription factor that regulates cellular oxidative defense by promoting anti-oxidant gene transcription including HO-1, solute carrier family 7 membrane 11 (SLC7A11), and GPX4 [15]. Erastin, induces cell ferroptosis via modulating multiple molecules, such as the cystine-glutamate transport receptor and the voltage-dependent anion channel [16]. Nrf2 suppresses ferroptosis in various cell types by protecting from lethal ROS stress, including cardiovascular diseases [17,18]. However, in the case of protecting cardiomyocytes against the adverse effects of DOX, the induction of Nrf2 signaling is associated with DOX resistance in cancer cells [19].

Prostaglandins (PGs) are a class of bioactive metabolites derived from arachidonic acid, which is sequentially catalyzed by cyclooxygenase (COX)-1 and-2 and PG synthases to generate PGD_2, PGE_2, $PGF_{2\alpha}$, prostacyclin (PGI_2), and thromboxane A2 (TxA_2). PGs exert various physiological and pathophysiological functions by binding to their own G-protein-coupled receptors: DP1-2 for PGD_2, EP1-4 for PGE_2, FP for $PGF_{2\alpha}$, IP for PGI_2, and TP for TxA_2. PG signaling acts as a pivotal regulator in cardiac remodeling after myocardial injury by modulating the cardiac microenvironment, including macrophage-mediated angiogenesis, inflammation resolution, and stem cell regeneration [20–22]. Notably, we and others found that PG receptors such as DP2, IP, FP, EP1, and EP4 are also abundantly expressed in cardiomyocytes [6,23,24]. Activation of PGD_2/DP2 signaling promotes ER stress–induced cardiomyocyte apoptosis after myocardial infarction [6] while activation of EP4 or FP receptor facilitates cardiomyocyte hypertrophy [23,24], suggesting that PG signaling is indispensable for the intrinsic adaptation of cardiomyocytes under cardiac stress. However, whether PGs-mediated signaling is involved in DOX-induced cardiomyocyte ferroptosis remains unclear.

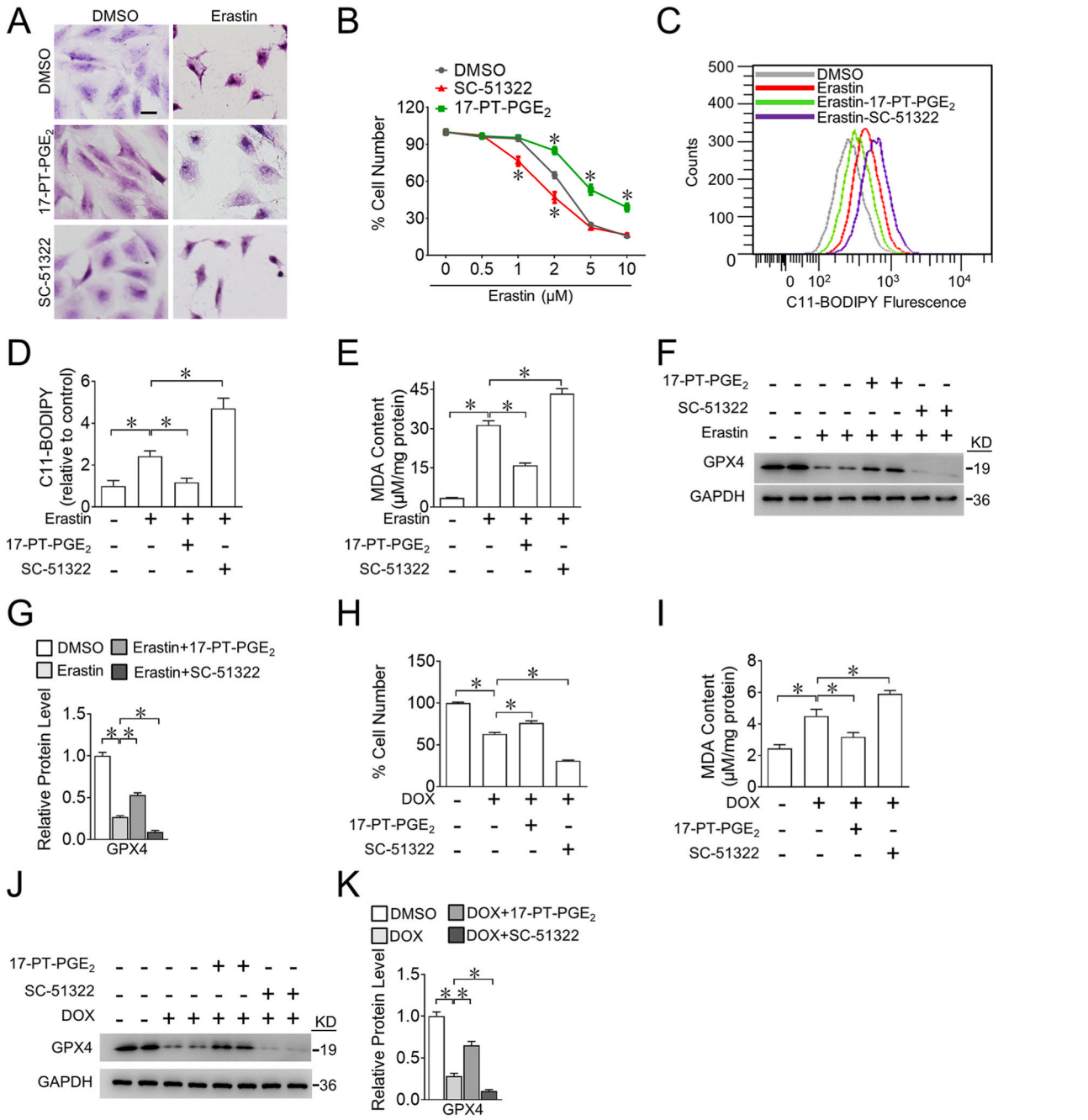

Fig. 2. Activation of EP1 inhibits DOX-induced ferroptosis in H9C2 cells

A. Representative H&E images of H9C2 cells treated with 17-PT-PGE$_2$ or SC-51322 in the presence of erastin. Scale bars: 20 μm

B. Effect of 17-PT-PGE$_2$ or SC-51322 on living H9C2 cells treated with different concentrations of erastin. *$P < 0.05$ vs DMSO; n = 4–6.

C. Representative flow cytometric plots showing intracellular ROS levels of H9C2 cells treated with 17-PT-PGE$_2$ or SC-51322 in the presence of erastin.

D. Quantification of ROS production in (C). *$P < 0.05$ vs indicated; n = 5.

E. MDA levels in H9C2 cells treated with 17-PT-PGE$_2$ or SC-51322 in the presence of erastin. *$P < 0.05$ vs indicated; n = 4.

F. Western blot analysis of GPX4 expression in H9C2 cells treated with 17-PT-PGE$_2$ or SC-51322 in the presence of erastin.

G. Quantification of relative protein expression levels of GPX4 in (F). *$P < 0.05$ as indicated; n = 4.

H. Effect of 17-PT-PGE$_2$ or SC-51322 of living H9C2 cells in the presence of DOX. *$P < 0.05$ vs DMSO; n = 8.

I. MDA levels in H9C2 cells treated with 17-PT-PGE$_2$ and SC-51322 in the presence of DOX. *$P < 0.05$ vs indicated; n = 4–5.

J. Western blot analysis of GPX4 expression in H9C2 cells treated with 17-PT-PGE$_2$ or SC-51322 in the presence of DOX.

K. Quantification of relative protein expression levels of GPX4 in (J) *$P < 0.05$ as indicated; n = 4.

Here we found that the PGE$_2$/EP1 axis was markedly upregulated in cardiomyocytes exposed to DOX and erastin. The EP1 inhibitor augmented whereas the EP1 agonist reduced DOX-induced cardiomyocyte ferroptosis. EP1 cardiac-specific knockout mice exhibited deteriorated myocardial function after DOX treatment. Loss of EP1 impaired Nrf2 activity in cardiomyocytes by suppressing Ca^{2+}/protein kinase C (PKC) signaling. Furthermore, EP1 activation also conferred protection against DOX-induced ferroptosis in human cardiomyocytes. Thus, the PGE$_2$/EP1 axis plays a crucial role in cardioprotection against DOX-induced cardiotoxicity.

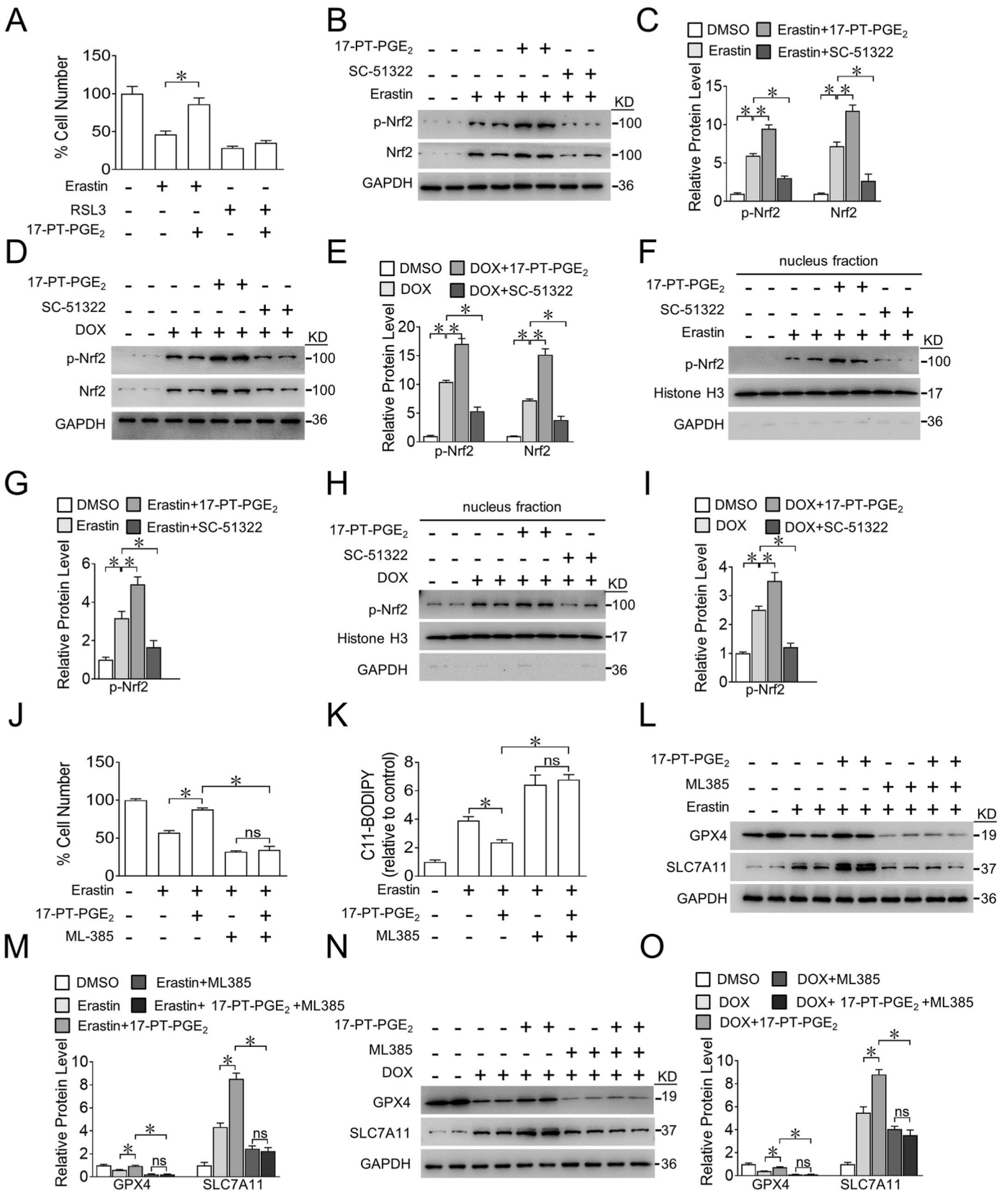

(caption on next page)

Fig. 3. EP1 activation reduces DOX-induced ferroptosis in cardiomyocytes through evoking Nrf2 activity
A. Effect of GPX4 inhibitor RSL3 on erastin-induced ferroptosis of H9C2 cells after17-PT-PGE_2 treatment. *$P < 0.05$ vs indicated; n = 8.
B. Western blot analysis of p-Nrf2 and Nrf2 expression in H9C2 cells treated with 17-PT-PGE_2 or SC-51322 in the presence of erastin.
C. Quantification of relative protein expression levels in (B). *$P < 0.05$ as indicated; n = 4.
D. Western blot analysis of p-Nrf2 and Nrf2 expression in H9C2 cells treated with 17-PT-PGE_2 or SC-51322 in the presence of DOX.
E. Quantification of relative protein expression levels in (D). *$P < 0.05$ as indicated; n = 4.
F. Western blot analysis of nuclear p-Nrf2 and Nrf2 expression in H9C2 cells treated with17-PT-PGE_2 or SC-51322 in the presence of erastin.
G. Quantification of relative protein expression levels in (F). *$P < 0.05$ as indicated; n = 4.
H. Western blot analysis of nuclear p-Nrf2 and Nrf2 expression in H9C2 cells treated with 17-PT-PGE_2 or SC-51322 in the presence of DOX.
I. Quantification of relative protein expression levels in (H). *$P < 0.05$ as indicated; n = 4.
J, K. Effect of ML-385 (5 μM) on cell viability (J) and intracellular ROS production (K) in H9C2 cells treated with 17-PT-PGE_2 in the presence of erastin. *$P < 0.05$ as indicated; (J), n = 8; (K), n = 6.
L. Western blot analysis of effect of ML-385 on the expression of GPX4 and SLC7A11 in H9C2 cells treated with 17-PT-PGE_2 in the presence of erastin.
M. Quantification of relative protein expression levels in (L). *$P < 0.05$ as indicated; n = 4.
N. Western blot analysis of effect of ML-385 on the expression of GPX4 and SLC7A11 in H9C2 cells treated with 17-PT-PGE_2 in the presence of DOX.
O. Quantification of relative protein expression levels in (N). *$P < 0.05$ as indicated; n = 4.

2. Materials and methods

2.1. Reagents

Doxorubicin (#T1020) was purchased from TargetMol (Wellesley Hills, MA, USA). 17-PT-PGE_2 (#14810) and SC-51322 (#10010744) were obtained from Cayman Chemical Company (Ann Arbor, MI, USA). U73122 (#U6756), and staurosporine (#539648) was obtained from Sigma Company (Sigma-Aldrich, St. Louis, MO, USA). Erastin (#S7242), RSL3 (#S8155), Fer-1 (#S7243), Nec-1s (#S8641), Bafilomycin A1 (#S1413), Z-VAD-FMK (#S7023), Trolox (#S3665), Deferoxamine mesylate (#S5742) and ML-385 (#S8790) were purchased from Selleck Chemicals (Houston, TX, USA). Wortmannin (#HY-10197), SP600125 (#HY-12041), and Ravoxertinib (#HY-15947) were purchased from MedChemExpress (MCE) Company (Shanghai, China).

2.2. Experimental animals

Eight-to ten-week-old male C57BL/6 mice were used in all experiments. $EP1^{flox/flox}$ mice (#020150) were obtained from Jackson Laboratories (Bar Harbor, ME, USA) [25]. HA-EP1 mice were generated by CRISPR/Cas9-mediated gene editing, where the HA tag was fused into N terminal of endogenous EP1 protein [26]. $EP1^{flox/flox}$ were crossed with MHC-Cre mice (Cre driven by α-myosin heavy chain [MHC] promoter) to generate cardiac-specific EP1 knockout mice ($EP1^{f/f}MHC^{Cre}$). The detailed primer sequences for genotyping are listed in Supplemental Table 1. All mice were maintained in the SPF animal laboratory of Tianjin Medical University in an environment with controlled temperature (22 ± 1 °C) and relative humidity (50 ± 5%) on a 12:12 h light/dark cycle, with free access to sterile food and water. All animal experiments were approved by the Institutional Animal Care and Use Committee of the Tianjin Medical University (Approval No: TMUaMEC 2020020) and performed according to the guidelines from the National Institutes of Health (NIH) Guide for the Care and Use of Laboratory Animals.

Mice were anesthetized with isoflurane inhalation. Specifically, mice were put into the induction chamber and 3–5% isoflurane was administrated until the animals were deeply anesthetized. During the construction of model, mice were given continuous inhalation of 1–2% isoflurane on the operating table to maintain surgical anesthesia. The DIC model was established as described previously [14]. Briefly, mice were subcutaneously injected with a single dose of DOX (10 mg/kg, dissolved in sterile saline) or saline at the indicated times. After DOX treatment for 7 days, mice were weighed and their cardiac functions were measured by echocardiography. The mice were deep anesthetized with 3% isoflurane and blood samples were collected, then euthanized under deep anesthesia by perfusing phosphate buffered saline into the hearts and heart samples were collected for further analysis. Fer-1 (1 mg/kg, dissolved in sterile saline) or vehicle was injected subcutaneously daily one day before DOX treatment.

Cardiac function was evaluated as previously described [6]. Echocardiographic data were obtained using a Vevo 2100 ultrasonography system (Visual Sonics Inc., Toronto, Canada) equipped with an MS400 linear array transducer.

2.3. Histological analysis

Mouse heart tissue samples were fixed in 4% paraformaldehyde and embedded in paraffin. Tissue sections of 5 μm thickness, hematoxylin and eosin (H&E), and Sirius Red staining were performed as previous described [14]. Cross-sectional area percentage of collagen was calculated using Image Pro Plus Software 6.0 (Media Cybernetics, CA, USA).

2.4. Cell line culture

H9C2 rat cardiomyocytes and AC16 human cardiomyocytes were maintained in Dulbecco's modified Eagle's medium (C11995500BT, DMEM; Gibco) supplemented with 10% (vol/vol) fetal bovine serum (1600044, FBS; Gibco) and 50 μg/mL penicillin-streptomycin (15240062; Gibco). Cells were incubated at 37 °C in a humidified atmosphere containing 5% CO_2. Cells were treated with erastin or DOX for 16–24 h for further analysis.

2.5. Primary cell isolation and culture

Primary cardiomyocytes and cardiac fibroblasts from rodents were isolated and cultured as our previously described [6]. Briefly, neonatal hearts (P1-3) were harvested and primary cardiomyocytes were isolated by Neonatal Rat/Mouse Cardiomyocyte Isolation Kit (Cellutron Life Technologies, MD, USA). Neonatal hearts were cut into small piecesand were plated on 0.1% gelatin-coated dishes in fibroblast medium. 7 days later, migrated fibroblasts were harvested by filtering through 40 μm cell strainers (Thermo Scientific).

Macrophages were collected by intraperitoneally injected with 2 mL 3% Brewer's thioglycolate as our described previously [21]. Macrophages were allowed to adhere in RPMI 1640 supplemented with 10% fetal bovine serum and non-adherent cells were removed.

2.6. PG extraction and analysis

H9C2 cells were treated with erastin or DOX, then incubated with arachidonic acid (30 μM) for 30 min, and culture supernatants (500 μL) were collected for PG extraction after protein quantification as previously described [6]. Briefly, after adding an internal standard, citric acid, and butylated hydroxytoluene, the samples were vigorously vortexed with 1 mL of solvent (normal hexane: ethyl acetate, 1:1) for 1 min and then centrifuged at 6000×*g* for 10 min. The supernatant (organic phase) was collected, dried under a gentle stream of nitrogen, and

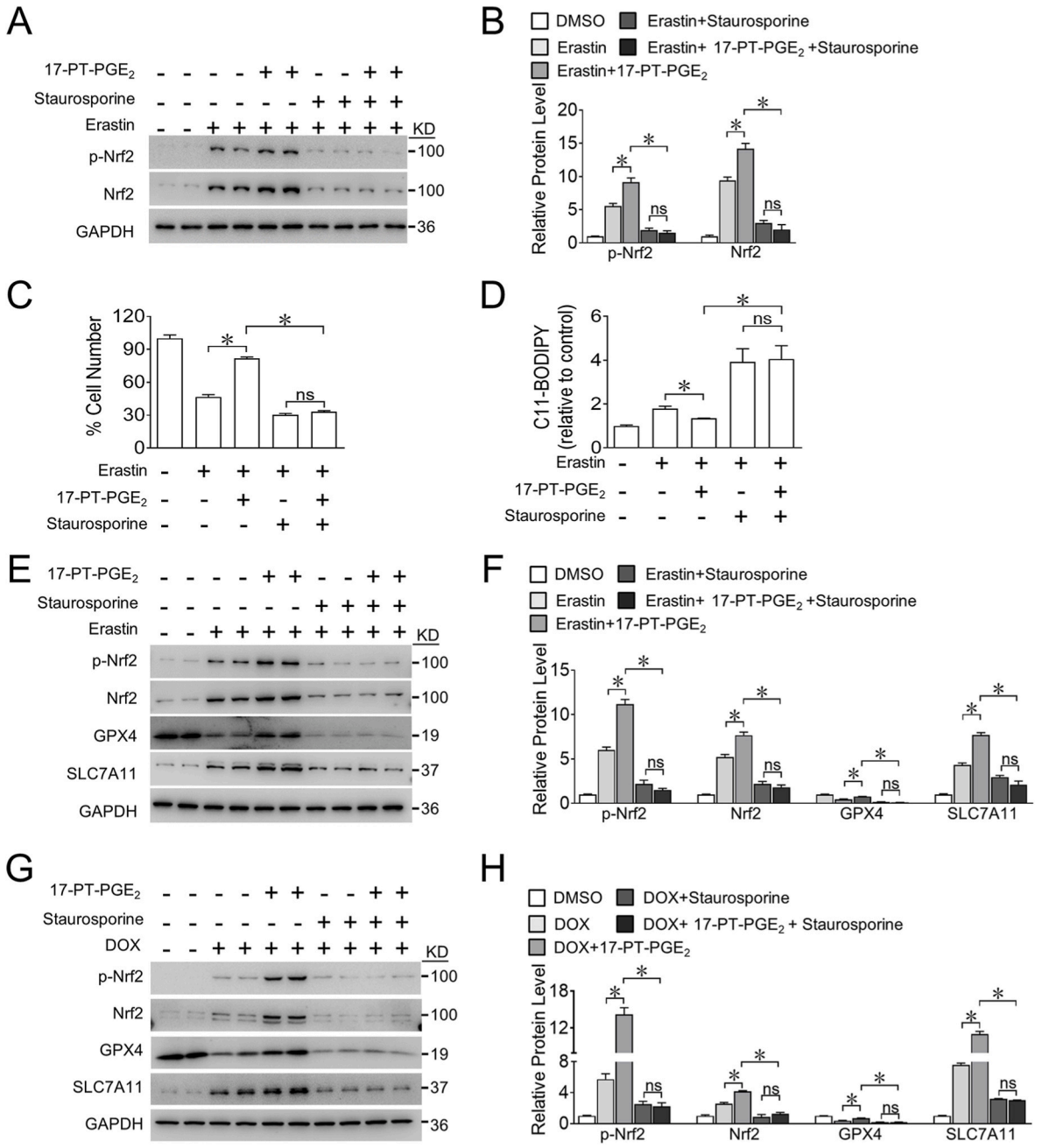

Fig. 4. Blockage of PKC abolishes EP1-mediated anti-ferroptosis effect on DOX-treated cardiomyocytes through suppressing Nrf2

A. Western blot analysis of effect of staurosporine (20 nM) on the expression of p-Nrf2 and Nrf2 in H9C2 cells treated with 17-PT-PGE_2 in the presence of erastin.

B. Quantification of relative protein expression levels in (A). *$P < 0.05$ as indicated; n = 4.

C, D. Effect of staurosporine on the cell viability (C) and intracellular ROS production (D) in H9C2 cells treated with 17-PT-PGE_2 in the presence of erastin. *$P < 0.05$ as indicated; (C), n = 8; (D), n = 7.

E. Western blot analysis of effect of staurosporine on the expression of p-Nrf2, Nrf2, GPX4 and SLC7A11 in H9C2 cells treated with17-PT-PGE_2 in the presence of erastin.

F. Quantification of relative protein expression levels in (E). *$P < 0.05$ as indicated; n = 4.

G. Western blot analysis of effect of staurosporine on the expression of p-Nrf2, Nrf2, GPX4 and SLC7A11 in H9C2 cells treated with 17-PT-PGE_2 in the presence of DOX.

H. Quantification of relative protein expression levels in (G). *$P < 0.05$ as indicated; n = 4.

dissolved in 100 μL 10% acetonitrile in water. Prostanoid metabolites were quantified using liquid chromatography–tandem mass spectrometry. PG levels were normalized to the total protein concentration.

2.7. Cell counting and viability assay

A Cell Counting Kit 8 (CCK-8) (C0038; Beyotime, Shanghai, China) was used. Briefly, cells were seeded into 96-well plates at a density of 5 × 10^3 cells/well and cultured for 24 h. After treatment with the indicated reagents for 24 h, CCK-8 solutions (10 μL) were added to each well and incubated for 2–3 h at 37 °C. Absorbance at a wavelength of 450 nm was measured using EnSpire Multimode Plate Reader (PerkinElmer, USA).

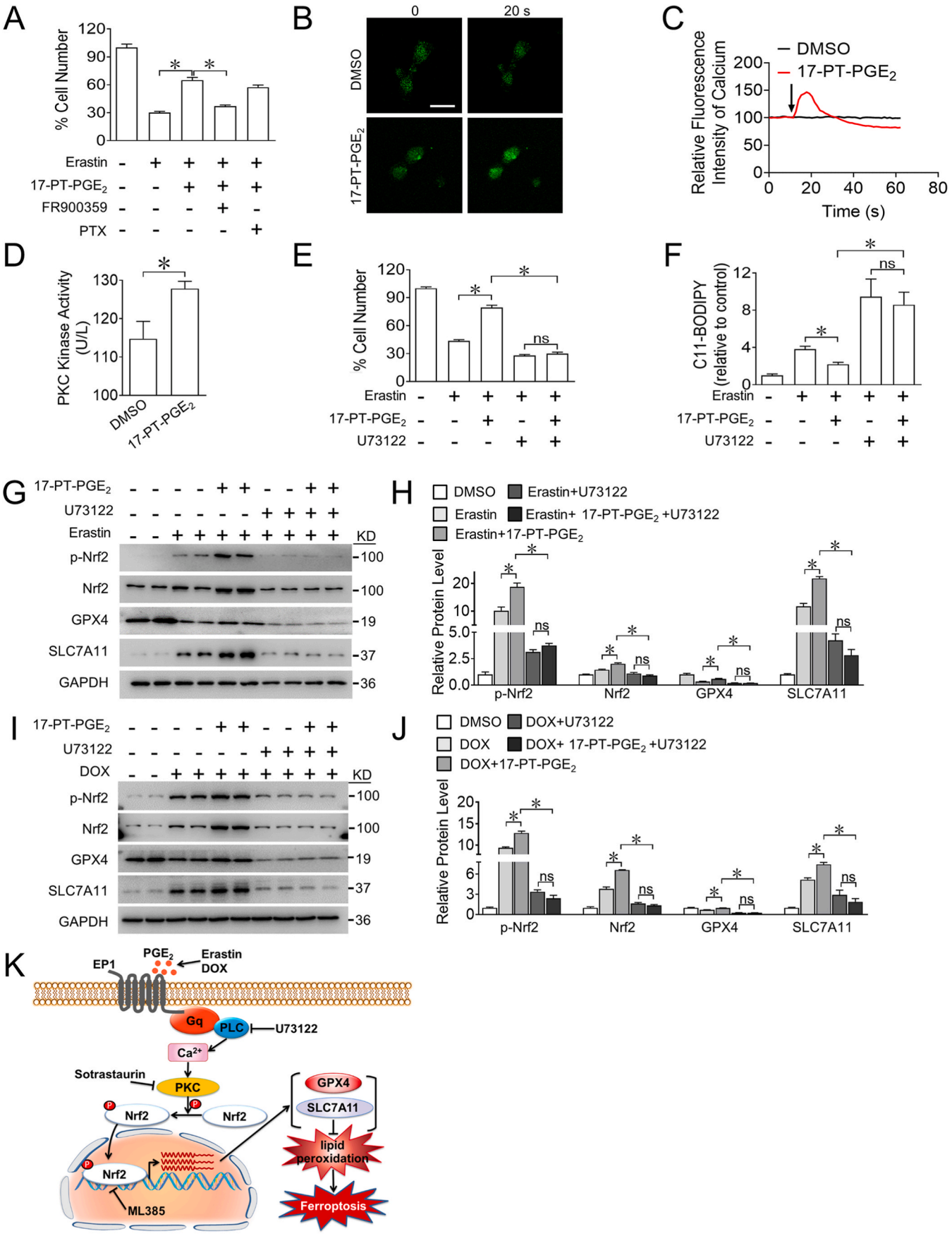

(caption on next page)

Fig. 5. EP1 activation protects cardiomyocytes from DOX-induced ferroptosis by mobilizing Ca^{2+} to activate PKC/Nrf2 signaling
A. Effect of FR900359 (1 μM) or PTX (10 μM) on the cell viability of H9C2 cells treated with 17-PT-PGE_2 in the presence of erastin. *$P < 0.05$ as indicated; n = 8.
B. Representative fluorescence images showing the intracellular Ca^{2+} spark in neonatal rat cardiomyocytes treated with 17-PT-PGE_2. Scale bars: 10 μm
C. The intracellular Ca^{2+} flux in neonatal rat cardiomyocytes treated with 17-PT-PGE_2. The arrow indicates the injection of 17-PT-PGE_2.
D. PKC kinase activity in H9C2 cells after 17-PT-PGE_2 treatment. *$P < 0.05$ as indicated; n = 5–6.
E, F. The effect of U73122 (5 μM) on the cell viability (E) and intracellular ROS production (F) in H9C2 cells treated with 17-PT-PGE_2 in the presence of erastin. *$P <$ 0.05 as indicated; E, n = 8; F, n = 5–6.
G. Western blot analysis of effect of U73122 on the expression of p-Nrf2, Nrf2, GPX4 and SLC7A11 in H9C2 cells treated with 17-PT-PGE_2 in the presence of erastin.
H. Quantification of relative protein expression levels in (G). *$P < 0.05$ as indicated; n = 4.
I. Western blot analysis of effect of U73122 on the expression of p-Nrf2, Nrf2, GPX4 and SLC7A11 in H9C2 cells treated with 17-PT-PGE_2 in the presence of DOX.
J. Quantification of relative protein expression levels in (I). *$P < 0.05$ as indicated; n = 4.
K. Schematic illustration of EP1-mediated myocardial protection in DOX-induced cardiomyocytes ferroptosis through Ca^{2+}/PKC/Nrf2 signaling pathway.

2.8. Quantitative real-time polymerase chain reaction

Total ribonucleic acid (RNA) was isolated from tissues or H9C2 cells by using TRIzol reagent (15596018; Invitrogen Life Technologies, Carlsbad, CA, USA) according to the manufacturer's instructions. Next, cDNA was synthesized from 1 μg of total RNA using a Hifair® III 1st Strand cDNA Synthesis Kit (11141ES60; Yeasen, Shanghai, China). Quantitative real-time PCR (qRT-PCR) was performed using SYBR Green (11201ES08; Yeasen, Shanghai, China) as previously described [27]. GAPDH was used as an endogenous control. The primer sequences used are listed in Supplemental Table 2.

2.9. Western blot analysis

Tissue protein was prepared in lysis buffer with a protease and phosphatase inhibitors cocktail (TargetMol, Wellesley Hills, MA, USA). The total protein content was determined using the Pierce™ BCA Protein Assay Kit (Thermo Fisher Scientific, Waltham, MA, USA) following the manufacturer's protocol. The proteins were denatured and resolved using 10% sodium dodecyl sulfate–polyacrylamide gel electrophoresis and transferred to a nitrocellulose membrane. The membranes were then blocked with 5% non-fat milk for 2 h at room temperature and incubated with specific primary antibodies at 4 °C overnight. Following incubation with horseradish peroxidase–conjugated secondary antibodies (1:2000; Cell Signaling Technology) for 2 h at room temperature, and the bands were detected using an enhanced chemiluminescence assay (Thermo Fisher Scientific). The primary antibodies used for western blotting were anti-HA (#3724, 1:1000; Cell Signaling Technology), anti-Nrf2 (A1244, 1:1000; Abclonal Technology), anti-p-Nrf2 (AP1133, 1:1000; Abclonal Technology), anti-SLC7A11 (A13685, 1:1000; Abclonal Technology), anti-MLKL (A21894, 1:1000; Abclonal Technology), anti-p-MLKL (AP1173, 1:1000; Abclonal Technology), anti-GPX4 (A11243, 1:1000; Abclonal Technology), anti-GAPDH (10494-1-AP, 1:10000; Proteintech), and histone H3 (4499, 1:1000; Cell Signaling Technology).

2.10. C11-BODIPY assay

Cells in 6-well plates were treated with different compounds for 16 h, and then cells washed with PBS and stained with C11-BODIPY (Abclonal, RM02821) at 37 °C for 1 h. Then, cells were dissociated by trypsinization after wash, and the fluorescent density of cells was detected using flow cytometer (BD Biosciences, USA) for C11-BODIPY 581/591 detection. The data were analyzed using FlowJo software (Tree Star Inc., Ashland, OR, USA).

2.11. Malondialdehyde (MDA) measurements

The concentration of MDA in cells, serum and mouse hearts was detected using the corresponding kits (S0131 M; Beyotime) according to the manufacturer's instructions. MDA concentrations were normalized to the corresponding protein concentrations, which were detected by the bicinchoninic acid assay method using a Pierce™ BCA Protein Assay kit.

2.12. Calcium imaging

Ca^{2+} imaging in cardiomyocytes was performed using Fluo-3-AM (121714-22-5, DojinDo Laboratories, Kumamoto, Japan). Cultured neonatal rat cardiomyocytes were preincubated in Hank's balanced salt solution (Invitrogen, Carlsbad, CA, USA) containing 3 μg/mL Fluo-3-AM as previously described [6]. After EP1 agonist stimulation, a series of images was captured every 50 ms using a laser-scanning confocal microscope (Carl Zeiss, Oberkochen, Germany). The recorded images were analyzed and quantified using ImageJ software (National Institutes of Health).

2.13. Cell death and membrane permeability assays

Cell death was analyzed by Trypan blue dye (ST798; Beyotime, Shanghai, China) according to the manufacture protocol. Briefly, cells were treated with indicated drugs for 24 h, then harvested using trypsin and stained with 0.4% Trypan blue dye for 3 min. The staining images was captured by light microscope (Leica DM IL LED, Germany) on a cell counting chamber.

Cell membrane permeability was examined by the cell-impermeable dye Sytox Green dye (S7020, Thermo Fisher) according to manufacturer's instructions. In brief, cells in 6-well plates were treated with indicated drugs for 24 h, then trypsinized, and stained with Sytox Green dye for 10 min after wash. The cells were fixed and analyzed by a flow cytometer (BD Biosciences, USA).

2.14. Statistical analyses

All data are shown as mean ± standard error of the mean (SEM). All data were tested using the Shapiro–Wilk normality test and were normally distributed. Comparisons between the two groups were analyzed using Mann–Whitney *U* test. Single-factor multiple group comparisons were performed using one-way analysis of variance (ANOVA) test followed by Tukey's test for normally distributed data or Welch ANOVA followed by Tamhane's T2 test for non-normally distributed data. Two-factor multiple group comparisons were performed using two-way ANOVA followed by Tukey's test. Data were analyzed using GraphPad Prism 8 (GraphPad Software Inc., San Diego, CA, USA). Statistical significance was set at $p < 0.05$.

3. Results

3.1. PGE_2/EP1 axis was activated in DOX-induced cardiomyocyte ferroptosis

To determine the role of PG signaling in DOX-induced cardiomyocyte ferroptosis, we first verified whether ferroptosis was involved in DOX-induced cardiomyocyte death. CCK-8 assays showed that ferroptosis inhibitors, such as Fer-1, deferoxamine mesylate (DFO; an iron chelator), and Trolox (a cell-permeable water-soluble derivative of vitamin E with potent antioxidant properties) reduced DOX-induced cell death by approximately 50% in the cardiomyocyte cell line H9C2

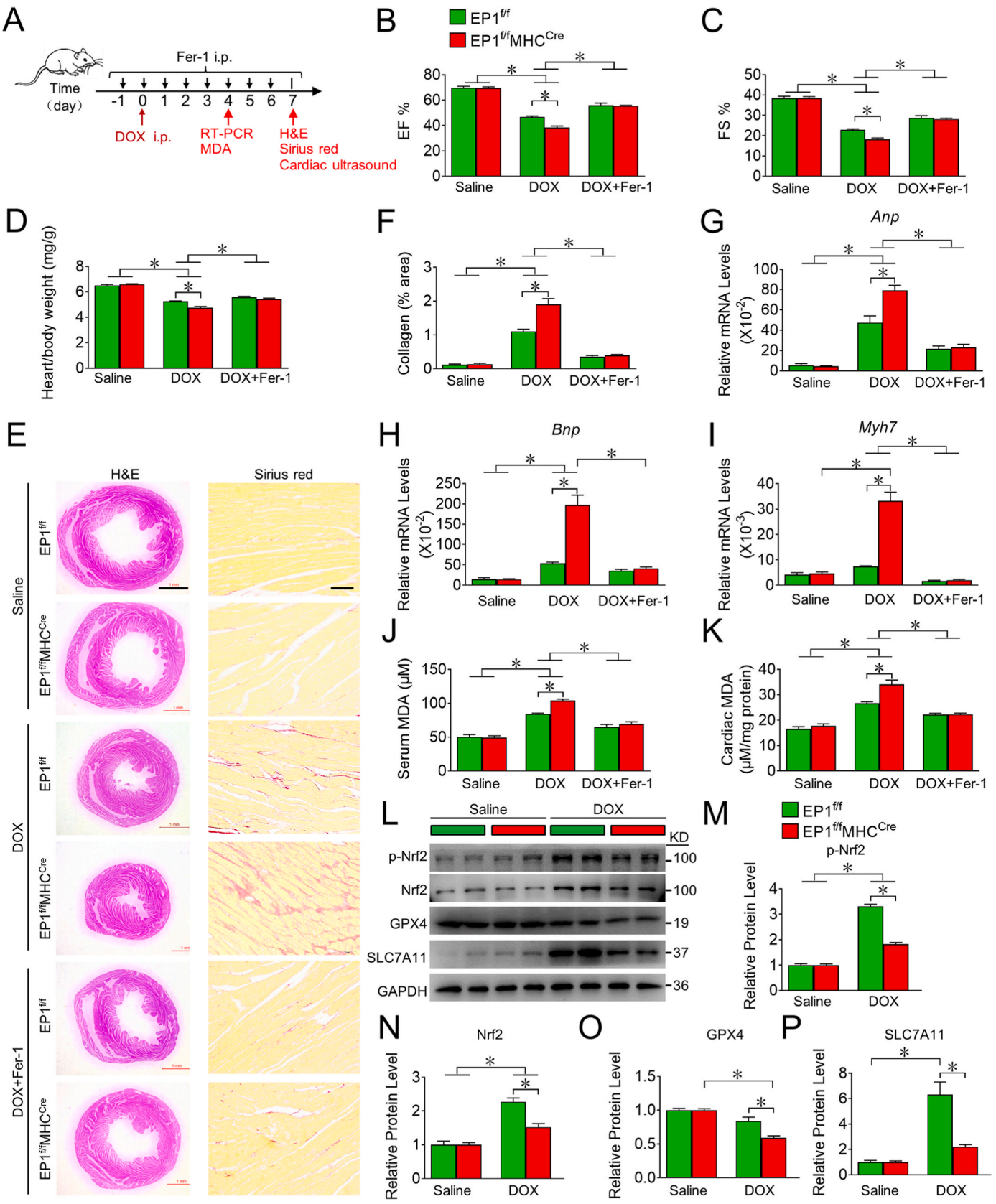

(caption on next page)

Fig. 6. EP1 deletion in cardiomyocytes exacerbates DOX-induced cardiac injury in mice through promoting cardiac ferroptosis
A. Schematic diagram of the treatment of Fer-1 in DOX-challenged mice.
B, C. Quantitative analysis of cardiac EF (B) and FS (C) in $EP1^{f/f}$ and $EP1^{f/f}MHC^{Cre}$ mice treated with DOX in the presence or absence of Fer-1. $^*P < 0.05$ vs indicated; n = 8.
D. The heart/body weight ratio of $EP1^{f/f}$ and $EP1^{f/f}MHC^{Cre}$ mice treated with DOX in the presence or absence of Fer-1. $^*P < 0.05$ vs indicated; n = 8.
E. Representative images of H&E and Sirius red staining of heart form $EP1^{f/f}$ and $EP1^{f/f}MHC^{Cre}$ mice treated with DOX in the presence or absence of Fer-1. H&E Scale bars: 1 mm; Sirius red Scale bars: 50 μm
F. Quantification of collagen content in (E). $^*P < 0.05$ vs indicated; n = 8.
G, I. The gene expressions of *Anp* (G), *Bnp* (H), *Myh7* (I) in the cardiac tissue from $EP1^{f/f}$ and $EP1^{f/f}MHC^{Cre}$ mice treated with DOX in the presence or absence of Fer-1. $^*P < 0.05$ vs indicated; (G), n = 8; (H), n = 5–8; (I), n = 5–8.
J, K. MDA levels in the serum (J) and cardiac tissue (K) from $EP1^{f/f}$ and $EP1^{f/f}MHC^{Cre}$ mice treated with DOX in the presence or absence of Fer-1. $^*P < 0.05$ vs indicated; (J), n = 6; (K), n = 5–8.
L. Western blot analysis of p-Nrf2, Nrf2, GPX4 and SLC7A11 expression in cardiac tissues from DOX-treated $EP1^{f/f}$ and $EP1^{f/f}MHC^{Cre}$ mice.
M-P. Quantification of protein expression of p-Nrf2 (M), Nrf2 (N), GPX4 (O), SLC7A11 (P) in (L). $^*P < 0.05$ as indicated; n = 6. (For interpretation of the references to colour in this figure legend, the reader is referred to the Web version of this article.)

(Fig. 1A), whereas necrostatin-1 (Nec-1s), a necroptosis inhibitor, and bafilomycin A1 (Baf-A1), an autophagy inhibitor, had no obvious effect on DOX-induced cell death, suggesting that ferroptosis was a major form of DOX-induced cell death. As expected, ferroptosis inducer erastin-induced cell death could be fully rescued by Fer-1, DFO, and Trolox (Fig. 1B and Supplemental Fig. 1), indicating that erastin induced ferroptosis rather than apoptosis, necrosis, or autophagy in H9C2 cells. Furthermore, we observed that PGE_2 and PGD_2 were the major PGs in cultured H9C2 cells and that stimulation with erastin and DOX dramatically enhanced PGE_2 and PGD_2 synthesis (Fig. 1C), and erastin treatment significantly upregulated the expression of their receptor subtypes, EP1 and DP2 in H9C2 cells, respectively (Fig. 1D). Interestingly, among all PG receptor agonists, only the EP1 agonist 17-phenyl-trinor-(pt)-PGE_2 (17-PT-PGE_2) markedly rescued erastin-induced ferroptotic cell death in H9C2 cells (Fig. 1E). Moreover, erastin gradually upregulated EP1 expression in H9C2 cells over time (Fig. 1F), and DOX promoted EP1 gene expression in a dose-dependent manner (Fig. 1G). Consistently, EP1 was also significantly elevated in erastin- or DOX-challenged neonatal rat cardiomyocytes (Supplemental Figs. 2A–B). To further elucidate EP1 expression during cardiac stress in vivo, we constructed mice with a hemagglutinin (HA) tag fused at the N-terminus of EP1 (EP1-HA) (Supplemental Fig. 3) and found that EP1 protein expression was significantly increased in the heart tissues of DOX-treated EP1-HA mice (Fig. 1H and I). These results indicate that PGE_2/EP1 signaling may be implicated in DOX-induced cardiomyocyte ferroptosis.

3.2. EP1 activation attenuates DOX-induced cardiomyocyte ferroptosis

To further investigate the role of EP1 in cardiomyocyte ferroptosis, we evaluated cytological changes in ferroptotic cardiomyocytes after pharmacological manipulation of EP1. The EP1 agonist 17-PT-PGE_2 prevented erastin-triggered cell shrinkage, whereas the EP1 antagonist SC-51322 accelerated erastin-induced cell shrinkage in H9C2 cells (Fig. 2A). Accordingly, EP1 activation markedly reduced, whereas EP1 inhibition increased erastin-induced H9C2 cell death (Fig. 2B). The EP1 agonist 17-PT-PGE_2 also markedly suppressed erastin-evoked ROS accumulation (Fig. 2C and D) and lipid peroxidation-derived malondialdehyde (MDA) generation (Fig. 2E) by upregulation of GPX4 protein expression in erastin-treated H9C2 cells (Fig. 2F and G), whereas the EP1 antagonist SC-51322 had the opposite effects (Fig. 2C–G). Similarly, EP1 activation mitigated DOX-induced cell death (Fig. 2H) by reducing MDA (Fig. 2I) and preventing GPX4 decrease (Fig. 2J and K), whereas EP1 inhibition accelerated DOX-induced cell death by increasing MDA levels and suppressing GPX4 expression in H9C2 cells (Fig. 2H–K). Similarly, the impacts of EP1 activation or inhibition on DOX- or erastin-induced cell death were also observed in neonatal rat cardiomyocytes (Supplemental Fig. 4). Thus, the activation of EP1 protects cardiomyocytes against DOX-induced cardiotoxicity by suppressing cardiomyocyte ferroptosis.

3.3. EP1 suppresses DOX-induced cardiomyocyte ferroptosis by enhancing Nrf2 activity

Next, we explored the mechanisms underlying EP1-mediated ferroptosis in cardiomyocytes. We observed that 17-PT-PGE_2 treatment reduced H9C2 cell death induced by erastin, not by GPX4 inhibitor RSL3 (Fig. 3A), suggesting a crucial role of GPX4 in EP1-mediated protection against cardiomyocyte ferroptosis. Both the mRNA and protein expression of GPX4 were markedly upregulated in erastin-treated H9C2 cells by the EP1 agonist 17-PT-PGE_2 and suppressed by the EP1 inhibitor SC-51322 (Fig. 2F and Supplemental Fig. 5), indicating that EP1 may modulate GPX4 expression at the transcriptional level. We then examined changes in Nrf2, a classical transcription factor that drives GPX4 gene expression and suppresses ferroptosis [28,29]. As expected, Nrf2 was activated by EP1 agonist and repressed by EP1 inhibitor in erastin-treated H9C2 cells, as determined by the levels of phosphorylated Nrf2 (Fig. 3B and C). Similar results for Nrf2 were also observed in DOX-treated H9C2 cells (Fig. 3D and E). Moreover, the activation of EP1 promoted the nuclear translocation of Nrf2 in erastin- or DOX-treated H9C2 cells, whereas EP1 inhibitor had the opposite effect (Fig. 3F–I). Nrf2 inhibition abolished 17-PT-PGE_2-conferred protection against erastin-induced cell death in H9C2 cells (Fig. 3J) as evidenced by increased ROS accumulation (Fig. 3K) and reduced GPX4 and SLC7A11 expression in erastin-exposed H9C2 cells (Fig. 3L and M). Likewise, inhibition of Nrf2 also abrogated the 17-PT-PGE_2-induced increase in GPX4 and SLC7A11 levels in DOX-treated H9C2 cells (Fig. 3N and O). Thus, activation of EP1 protects cardiomyocytes from DOX-induced ferroptosis through activation of Nrf2.

3.4. EP1 protects cardiomyocytes from DOX-induced ferroptosis by activating PKC/Nrf2 signaling

Nrf2 can be activated by various protein kinases, including protein kinase C (PKC), phosphatidylinositol 3-kinase (PI3K), c-Jun NH2-terminal kinase (JNK), and extracellular signal-regulated protein kinase (ERK) [30]. We found that the PKC inhibitor staurosporine, but not inhibitors of PI3K, JNK, and ERK, markedly suppressed the increased phosphorylation of Nrf2 induced by the EP1 agonist in erastin-treated H9C2 cells (Fig. 4A and B and Supplemental Fig. 6). Importantly, PKC inhibition abrogated 17-PT-PGE_2-conferred protection against erastin-induced cell death by increasing ROS generation in H9C2 cells (Fig. 4C and D) and abolished 17-PT-PGE_2-induced increase of Nrf2 activity as well as GPX4 and SLC7A11 expression in both erastin- and DOX-treated H9C2 cells (Fig. 4E–H). These results indicate that EP1 activates the PKC/Nrf2 signaling pathway to reduce DOX-induced ferroptosis in cardiomyocytes.

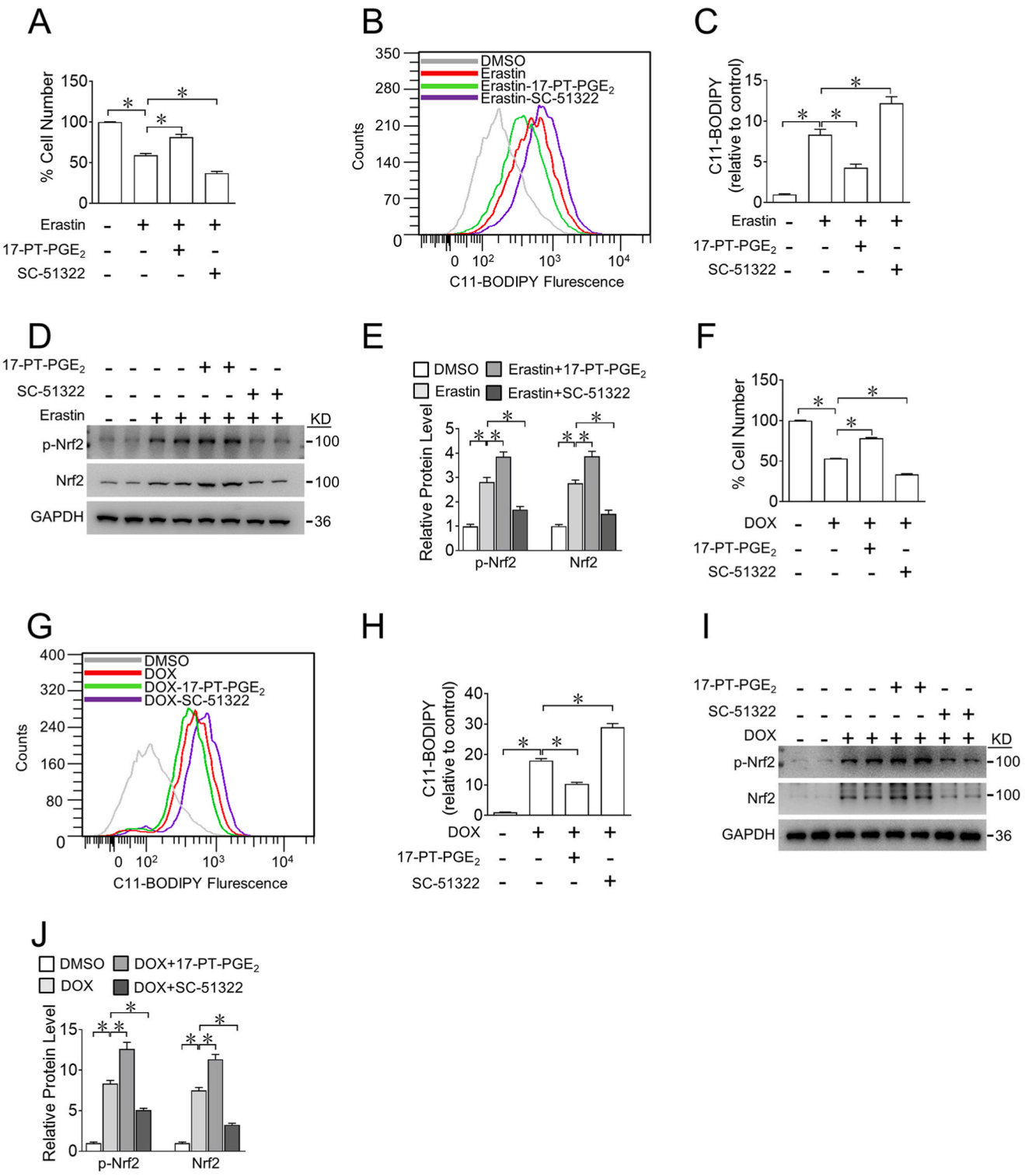

Fig. 7. EP1 activation prevents DOX-induced ferroptosis in human cardiomyocytes

A. Cell viability of AC16 cells treated with 17-PT-PGE$_2$ (2.5 μM) or SC-51322 (10 μM) in the presence of erastin (5 μM). *$P < 0.05$ vs indicated; n = 8.

B. Representative flow cytometric plots showing the intracellular ROS levels in AC16 cells treated with 17-PT-PGE$_2$ or SC-51322 in the presence of erastin.

C. Quantification of ROS production in (B). *$P < 0.05$ vs indicated; n = 5–8.

D. Western blot analysis of p-Nrf2 and total Nrf2 expression in AC16 cells treated with 17-PT-PGE$_2$ or SC-51322in the presence of erastin.

E. Quantification of relative protein expression levels in (D). *$P < 0.05$ as indicated; n = 4.

F. Cell viability of AC16 cells treated with 17-PT-PGE$_2$ or SC-51322 in the presence of DOX. *$P < 0.05$ vs indicated; n = 8.

G. Representative flow cytometric plots showing the intracellular ROS levels in AC16 cells treated with 17-PT-PGE$_2$ or SC-51322 in the presence of DOX.

H. Quantification of ROS production in (G). *$P < 0.05$ vs indicated; n = 6.

I. Western blot analysis of p-Nrf2 and total Nrf2 expression in AC16 cells treated with 17-PT-PGE$_2$ or SC-51322 in the presence of DOX.

J. Quantification of relative protein expression levels in (I). *$P < 0.05$ as indicated; n = 4.

3.5. EP1 alleviates DOX-induced cardiomyocyte ferroptosis by triggering Ca^{2+}/PKC-mediated Nrf2 activity

As a G protein-coupled receptor, EP1 couples with $G_{\alpha q}/Ca^{2+}$ or $G_{\alpha i}$/cAMP to activate various downstream signalings [31,32]. Notably, the EP1 agonist-conferred cardiomyocyte protection against ferroptosis was selectively abolished by the $G_{\alpha q}$ inhibitor FR900359 in H9C2 cells (Fig. 5A). A dramatic increase in Ca^{2+} flux was observed in the 17-PT-PGE_2-treated neonatal rat cardiomyocytes (Fig. 5B and C). Since intracellular Ca^{2+} collaborates with diacylglycerol (DAG) to trigger PKC stimulation, we examined whether the activation of EP1 could elicit changes in PKC activity in cardiomyocytes and found that treatment with 17-PT-PGE_2 significantly upregulated PKC activity in H9C2 cells (Fig. 5D). Blockage of Ca^{2+} flux with the PLC inhibitor U73122 abrogated the 17-PT-PGE_2-conferred cardiomyocyte protection against ferroptosis by increasing ROS accumulation in erastin-treated H9C2 cells (Fig. 5E and F). Consistently, inhibition of Ca^{2+} also abolished EP1 agonist-induced increase of Nrf2 activity and GPX4 and SLC7A11 expression in both erastin- and DOX-treated H9C2 cells (Fig. 5G–J). Collectively, activation of EP1 reduced erastin-or DOX-induced ferroptosis in cardiomyocytes through the Ca^{2+}/PKC/Nrf2 signaling pathway (Fig. 5K).

3.6. Depletion of EP1 in cardiomyocytes aggravates DOX-induced cardiomyopathy in mice

PGE_2 production is markedly increased in heart tissues in response to DOX treatment [33]. To verify EP1-mediated anti-ferroptosis in cardiomyocytes in vivo, we generated cardiac-specific EP1 knockout mice ($EP1^{f/f}MHC^{Cre}$) (Supplemental Figs. 7A and B) and evaluated their cardiac functions after DOX treatment (Fig. 6A). We found that $EP1^{f/f}MHC^{Cre}$ mice exhibited deteriorated left ventricular function (Fig. 6B and C), lower heart/body weight ratios (Fig. 6D), excessive cardiac collagen deposition (Fig. 6E and F), and higher expression of cardiac stress genes such as atrial natriuretic peptide (Anp), brain natriuretic peptide (Bnp), and myosin heavy chain 7 (Myh7) (Fig. 6G–I), and higher MDA levels in serum and cardiac tissues (Fig. 6J and K), and decreased Nrf2, GPX4 and SLC7A11 expression in heart tissues (Fig. 6L-P) after DOX insult when compared to their littermate controls. EP1 deletion had no markedly influence on MLKL phosphorylation (the key marker of necrosis) in cardiac tissues, although DOX treatment increased cardiac necrosis in mice (Supplemental Fig. 7C). Treatment with the ferroptosis inhibitor Fer-1 significantly rescued DOX-induced cardiac dysfunction, fibrosis, and oxidative stress in $EP1^{f/f}MHC^{Cre}$ mice (Fig. 6B–K). Thus, loss of EP1 deteriorated DOX-induced cardiotoxicity by promoting cardiomyocyte ferroptosis in mice.

3.7. EP1 activation inhibits DOX-induced ferroptosis in human cardiomyocytes

To explore whether EP1 mediates anti-ferroptotic effect in human cardiomyocytes, we examined the effects of pharmacological manipulation of EP1 on erastin- or DOX-induced cell death in AC16 human cardiomyocytes. Again, the EP1 agonist markedly reduced, whereas the EP1 antagonist increased erastin-induced AC16 cell death (Fig. 7A). EP1 activation also reduced ROS accumulation (Fig. 7B and C) by promoting Nrf2 activation in erastin-treated AC16 cells (Fig. 7D and E), whereas inhibition of EP1 had the opposite effect (Fig. 7A–E). Consistently, EP1 activation attenuated DOX-induced AC16 cell death (Fig. 7F) by reducing ROS levels (Fig. 7G and H) and enhancing Nrf2 activity (Fig. 7I and J) in DOX-exposed AC16 cells, whereas inhibition of EP1 recapitulated the pro-ferroptotic phenotype in DOX-treated AC16 cells (Fig. 7F–J).

4. Discussion

The clinical application of DOX is restricted by its cardiotoxicity, and pharmacological interventions for reducing its cardiac side effects are still lacking. Here, we found that the PGE_2/EP1 axis is markedly upregulated during DOX-induced cardiomyocyte ferroptosis. EP1 activation protected cardiomyocytes from DOX-induced ferroptosis by upregulating anti-oxidative gene expression in a Ca^{2+}/PKC/Nrf2 signaling dependent manner. EP1 deficiency in cardiomyocytes promoted ferroptosis and aggravated DOX-induced myocardial injury in mice. Thus, targeting EP1 activation may represent a novel strategy for DIC treatment.

Ferroptosis has been implicated in the development of various cardiocerebral vascular diseases including DIC, cardiac ischemia/reperfusion injury, heart failure, atherosclerosis, and stroke [34,35]. The severity of myocardial infarction, atherosclerosis, and DIC is positively associated with the expression of COX-2 and oxidative insult [36–38]. Indeed, COX-2 has an initial adaptive role in attenuating injury, and its inhibition aggravates DOX-mediated cardiac ferroptosis [37] and increases the risk of myocardial infarction and heart failure [39,40]. The inhibition of COX with non-selective COX inhibitors, such as aspirin and ibuprofen, induces ferroptosis in cancer cells [41,42] and enhances the anti-tumor activity of DOX [43], indicating that COX-derived PGs may exert an anti-ferroptotic effect against oxidative damage. We found that PGE_2, one of the most abundant COX-2 derived PGs in cardiomyocytes, was dramatically increased in DOX-induced cardiac ferroptosis and conferred cardioprotective effects against DIC through the EP1 receptor. Myocardial specific knockout of EP1 significantly aggravated DIC in mice. In line with our results, PGE_2 attenuated cerebral I/R by suppressing ferroptosis through the reduction of lipid peroxidation [44] and improved outcomes following hemorrhagic stroke in mice [45]. Thus, the PGE_2/EP1 axis alleviates DIC by suppressing cardiac ferroptosis. Interestingly, meloxicam, a COX-2 inhibitor, protects heart against doxorubicin toxicity in tumor-bearing mice, probably through suppression of cardiac lipid peroxidation and inflammatory reaction [33].

Transcription factor Nrf2 plays a pivotal role in the control of redox balance and counteracts ferroptosis by promoting antioxidant gene transcription [18,46]. Activation of the Nrf2 signaling pathway protects against oxidative stress–induced cardiac injuries, including DIC, pressure overload–induced heart failure, and ischemia–reperfusion injury [5,47–50]. Under normal conditions, Kelch-like ECH-associated protein 1 (Keap1) interacts with Nrf2 and mediates its ubiquitination and degradation [51]. During oxidative stress, oxidized cysteine residues disrupt Keap1-Nrf2 interaction, leading to Nrf2 stabilization, nuclear translocation, and ultimately activation of cytoprotective antioxidant genes [52]. In HepG2 cells, oxidative stress drives PKC to phosphorylate Nrf2 at Ser 40, leading to Nrf2 dissociation from Keap1, thus promoting Nrf2 transcriptional activity [53,54]. In skeletal muscle cells, the inhibition of JNK decreases Nrf2 content and disrupts redox balance [55]. In cardiomyocytes, PI3K/Akt signaling evokes Nrf2 activity and protects against ROS-mediated apoptosis [56]. However, the upstream regulator of Nrf2 in DIC remains unclear. We observed that EP1 activation promoted nuclear Nrf2 activity and reduced DOX-induced ferroptosis in cardiomyocytes through PKC-mediated phosphorylation at Ser40. Indeed, PKC/Nrf2 signaling activated by ischemic postconditioning also provides cardioprotective effects against IR injury by maintaining the antioxidant defense system [57,58].

In summary, we found that the PGE_2/EP1 axis protected the heart from DIC by suppressing cardiomyocyte ferroptosis via the PKC/Nrf2 signaling pathway, and targeting EP1 may represent a promising strategy for prevention and treatment of chemotherapy-associated cardiomyopathy.

Author contributions

B.W., **S.Z.**, and **Y.Y.** devised the project. **B.W.** conducted most

experiments, **Y.J.** and **J.L.** contributed mouse experiments. **B.W.** drafted the manuscript, **Q.L.** provided reagents. **Y.S.**, **S.Z.**, and **Y.Y.** revised the manuscript. All authors have read and given permission to the paper.

Declaration of competing interest

The authors declare that there is no conflict of interest

Data availability

No data was used for the research described in the article.

Acknowledgements

This research was supported by the National Key R&D Program of China (2021YFC2701104, and 2021YFF0702103), National Natural Science Foundation of China (82030015, 82241016, 82261160656 and 82171792). Y. Y is Fellow at the Jiangsu Collaborative Innovation Center for Cardiovascular Disease Translational Medicine.

Appendix A. Supplementary data

Supplementary data to this article can be found online at https://doi.org/10.1016/j.redox.2023.102825.

References

[1] M.S. Ewer, S.M. Ewer, Cardiotoxicity of anticancer treatments, Nat. Rev. Cardiol. 12 (11) (2015) 620.
[2] Z. Raisi-Estabragh, O. Kobo, P. Freeman, S.E. Petersen, L. Kolman, R.J.H. Miller, A. Roguin, H.G.C. Van Spall, J. Vuong, E.H. Yang, M.A. Mamas, Temporal trends in disease-specific causes of cardiovascular mortality amongst patients with cancer in the USA between 1999 and 2019, Eur Heart J Qual Care Clin Outcomes 9 (1) (2022) 54–63.
[3] P.K. Singal, N. Iliskovic, Doxorubicin-induced cardiomyopathy, N. Engl. J. Med. 339 (13) (1998) 900–905.
[4] S. Zhang, X.B. Liu, T. Bawa-Khalfe, L.S. Lu, Y.L. Lyu, L.F. Liu, E.T.H. Yeh, Identification of the molecular basis of doxorubicin-induced cardiotoxicity, Nat. Med. 18 (11) (2012) 1639–1642.
[5] Y. Ichikawa, M. Ghanefar, M. Bayeva, R. Wu, A. Khechaduri, S.V. Naga Prasad, R. K. Mutharasan, T.J. Naik, H. Ardehali, Cardiotoxicity of doxorubicin is mediated through mitochondrial iron accumulation, J. Clin. Invest. 124 (2) (2014) 617–630.
[6] S. Zuo, D. Kong, C. Wang, J. Liu, Y. Wang, Q. Wan, S. Yan, J. Zhang, J. Tang, Q. Zhang, L. Lyu, X. Li, Z. Shan, L. Qian, Y. Shen, Y. Yu, CRTH2 promotes endoplasmic reticulum stress-induced cardiomyocyte apoptosis through m-calpain, EMBO Mol. Med. 10 (3) (2018), e8237.
[7] B.B. Hasinoff, E.H. Herman, Dexrazoxane: how it works in cardiac and tumor cells. Is it a prodrug or is it a drug? Cardiovasc. Toxicol. 7 (2) (2007) 140–144.
[8] S.M. Swain, F.S. Whaley, M.C. Gerber, S. Weisberg, M. York, D. Spicer, S.E. Jones, S. Wadler, A. Desai, C. Vogel, J. Speyer, A. Mittelman, S. Reddy, K. Pendergrass, E. Velez-Garcia, M.S. Ewer, J.R. Bianchine, R.A. Gams, Cardioprotection with dexrazoxane for doxorubicin-containing therapy in advanced breast cancer, J. Clin. Oncol. 15 (4) (1997) 1318–1332.
[9] F. Shaikh, L.L. Dupuis, S. Alexander, A. Gupta, L. Mertens, P.C. Nathan, Cardioprotection and second malignant neoplasms associated with dexrazoxane in children receiving anthracycline chemotherapy: a systematic review and meta-analysis, J. Natl. Cancer Inst. 108 (4) (2016) djv357.
[10] D.L. Friedman, J. Whitton, W. Leisenring, A.C. Mertens, S. Hammond, M. Stovall, S. S. Donaldson, A.T. Meadows, L.L. Robison, J.P. Neglia, Subsequent neoplasms in 5-year survivors of childhood cancer: the childhood cancer survivor study, J. Natl. Cancer Inst. 102 (14) (2010) 1083–1095.
[11] E. Christidi, L.R. Brunham, Regulated cell death pathways in doxorubicin-induced cardiotoxicity, Cell Death Dis. 12 (4) (2021) 339.
[12] J.C. Canzoneri, A.K. Oyelere, Interaction of anthracyclines with iron responsive element mRNAs, Nucleic Acids Res. 36 (21) (2008) 6825–6834.
[13] S. Kotamraju, C.R. Chitambar, S.V. Kalivendi, J. Joseph, B. Kalyanaraman, Transferrin receptor-dependent iron uptake is responsible for doxorubicin-mediated apoptosis in endothelial cells: role of oxidant-induced iron signaling in apoptosis, J. Biol. Chem. 277 (19) (2002) 17179–17187.
[14] X. Fang, H. Wang, D. Han, E. Xie, X. Yang, J. Wei, S. Gu, F. Gao, N. Zhu, X. Yin, Q. Cheng, P. Zhang, W. Dai, J. Chen, F. Yang, H.T. Yang, A. Linkermann, W. Gu, J. Min, F. Wang, Ferroptosis as a target for protection against cardiomyopathy, Proc. Natl. Acad. Sci. U. S. A. 116 (7) (2019) 2672–2680.
[15] X. Song, D. Long, Nrf2 and ferroptosis: a new research direction for neurodegenerative diseases, Front. Neurosci. 14 (2020) 267.
[16] Y. Zhao, Y. Li, R. Zhang, F. Wang, T. Wang, Y. Jiao, The role of erastin in ferroptosis and its prospects in cancer therapy, OncoTargets Ther. 13 (2020) 5429–5441.
[17] A. Anandhan, M. Dodson, C.J. Schmidlin, P. Liu, D.D. Zhang, Breakdown of an ironclad defense system: the critical role of NRF2 in mediating ferroptosis, Cell Chem. Biol. 27 (4) (2020) 436–447.
[18] M. Dodson, R. Castro-Portuguez, D.D. Zhang, NRF2 plays a critical role in mitigating lipid peroxidation and ferroptosis, Redox Biol. 23 (2019), 101107.
[19] S. Mirzaei, A. Zarrabi, F. Hashemi, A. Zabolian, H. Saleki, N. Azami, S. Hamzehlou, M.V. Farahani, K. Hushmandi, M. Ashrafizadeh, H. Khan, A.P. Kumar, Nrf2 signaling pathway in chemoprotection and doxorubicin resistance: potential application in drug discovery, Antioxidants 10 (3) (2021) 349.
[20] Y.C. Hsueh, J.M. Wu, C.K. Yu, K.K. Wu, P.C. Hsieh, Prostaglandin E(2) promotes post-infarction cardiomyocyte replenishment by endogenous stem cells, EMBO Mol. Med. 6 (4) (2014) 496–503.
[21] D. Kong, Y. Shen, G. Liu, S. Zuo, Y. Ji, A. Lu, M. Nakamura, M. Lazarus, C. A. Stratakis, R.M. Breyer, Y. Yu, PKA regulatory IIalpha subunit is essential for PGD2-mediated resolution of inflammation, J. Exp. Med. 213 (10) (2016) 2209–2226.
[22] J. Tang, Y. Shen, G. Chen, Q. Wan, K. Wang, J. Zhang, J. Qin, G. Liu, S. Zuo, B. Tao, Y. Yu, J. Wang, M. Lazarus, Y. Yu, Activation of E-prostanoid 3 receptor in macrophages facilitates cardiac healing after myocardial infarction, Nat. Commun. 8 (2017), 14656.
[23] J.Y. Qian, P. Harding, Y. Liu, E. Shesely, X.P. Yang, M.C. LaPointe, Reduced cardiac remodeling and function in cardiac-specific EP4 receptor knockout mice with myocardial infarction, Hypertension 51 (2) (2008) 560–566.
[24] P. Kunapuli, J.A. Lawson, J.A. Rokach, J.L. Meinkoth, G.A. FitzGerald, Prostaglandin F2alpha (PGF2alpha) and the isoprostane, 8, 12-iso-isoprostane F2alpha-III, induce cardiomyocyte hypertrophy. Differential activation of downstream signaling pathways, J. Biol. Chem. 273 (35) (1998) 22442–22452.
[25] M. Fritz, A.M. Klawonn, A. Nilsson, A.K. Singh, J. Zajdel, D.B. Wilhelms, M. Lazarus, A. Lofberg, M. Jaarola, U.O. Kugelberg, T.R. Billiar, D.J. Hackam, C. P. Sodhi, M.D. Breyer, J. Jakobsson, M. Schwaninger, G. Schutz, J.R. Parkitna, C. B. Saper, A. Blomqvist, D. Engblom, Prostaglandin-dependent modulation of dopaminergic neurotransmission elicits inflammation-induced aversion in mice, J. Clin. Invest. 126 (2) (2016) 695–705.
[26] X.X. Tao, B. Wang, S.K. Zuo, Y. Yu, [Identification of mouse lines with HA-tagged prostaglandin receptors], Sheng Li Xue Bao 73 (4) (2021) 559–570.
[27] S. Zuo, B. Wang, J. Liu, D. Kong, H. Cui, Y. Jia, C. Wang, X. Xu, G. Chen, Y. Wang, L. Yang, K. Zhang, D. Ai, J. Du, Y. Shen, Y. Yu, ER-anchored CRTH2 antagonizes collagen biosynthesis and organ fibrosis via binding LARP6, EMBO J. 40 (16) (2021), e107403.
[28] T. Tadokoro, M. Ikeda, T. Ide, H. Deguchi, S. Ikeda, K. Okabe, A. Ishikita, S. Matsushima, T. Koumura, K.I. Yamada, H. Imai, H. Tsutsui, Mitochondria-dependent ferroptosis plays a pivotal role in doxorubicin cardiotoxicity, JCI Insight 5 (9) (2020), e132747.
[29] W.S. Yang, R. SriRamaratnam, M.E. Welsch, K. Shimada, R. Skouta, V. S. Viswanathan, J.H. Cheah, P.A. Clemons, A.F. Shamji, C.B. Clish, L.M. Brown, A. W. Girotti, V.W. Cornish, S.L. Schreiber, B.R. Stockwell, Regulation of ferroptotic cancer cell death by GPX4, Cell 156 (1–2) (2014) 317–331.
[30] T. Liu, Y.F. Lv, J.L. Zhao, Q.D. You, Z.Y. Jiang, Regulation of Nrf2 by phosphorylation: consequences for biological function and therapeutic implications, Free Radic. Biol. Med. 168 (2021) 129–141.
[31] R. Ji, C.L. Chou, W. Xu, X.B. Chen, D.F. Woodward, J.W. Regan, EP1 prostanoid receptor coupling to G i/o up-regulates the expression of hypoxia-inducible factor-1 alpha through activation of a phosphoinositide-3 kinase signaling pathway, Mol. Pharmacol. 77 (6) (2010) 1025–1036.
[32] T.D. Bryson, P. Harding, Prostaglandin E2 EP receptors in cardiovascular disease: an update, Biochem. Pharmacol. 195 (2022), 114858.
[33] M.H. Hassan, H.A. El-Beshbishy, H. Aly, S.M. Attia, S.A. Bahashwan, M. M. Ghobara, Modulatory effects of meloxicam on cardiotoxicity and antitumor activity of doxorubicin in mice, Cancer Chemother. Pharmacol. 74 (3) (2014) 559–569.
[34] Y. Leng, X. Luo, J. Yu, H. Jia, B. Yu, Ferroptosis: a potential target in cardiovascular disease, Front. Cell Dev. Biol. 9 (2021), 813668.
[35] Y. Zhang, X. Lu, B. Tai, W. Li, T. Li, Ferroptosis and its multifaceted roles in cerebral stroke, Front. Cell. Neurosci. 15 (2021), 615372.
[36] Y. Zhou, H. Zhou, L. Hua, C. Hou, Q. Jia, J. Chen, S. Zhang, Y. Wang, S. He, E. Jia, Verification of ferroptosis and pyroptosis and identification of PTGS2 as the hub gene in human coronary artery atherosclerosis, Free Radic. Biol. Med. 171 (2021) 55–68.
[37] N.P. Dowd, M. Scully, S.R. Adderley, A.J. Cunningham, D.J. Fitzgerald, Inhibition of cyclooxygenase-2 aggravates doxorubicin-mediated cardiac injury in vivo, J. Clin. Invest. 108 (4) (2001) 585–590.
[38] F. Gao, Y. Zhao, B. Zhang, C. Xiao, Z. Sun, Y. Gao, X. Dou, Suppression of lncRNA Gm47283 attenuates myocardial infarction via miR-706/Ptgs2/ferroptosis axis, Bioengineered 13 (4) (2022) 10786–10802.
[39] M. Mamdani, D.N. Juurlink, D.S. Lee, P.A. Rochon, A. Kopp, G. Naglie, P.C. Austin, A. Laupacis, T.A. Stukel, Cyclo-oxygenase-2 inhibitors versus non-selective non-steroidal anti-inflammatory drugs and congestive heart failure outcomes in elderly patients: a population-based cohort study, Lancet 363 (9423) (2004) 1751–1756.
[40] B. Pitt, C. Pepine, J.T. Willerson, Cyclooxygenase-2 inhibition and cardiovascular events, Circulation 106 (2) (2002) 167–169.
[41] X. Gao, N. Guo, H. Xu, T. Pan, H. Lei, A. Yan, Y. Mi, L. Xu, Ibuprofen induces ferroptosis of glioblastoma cells via downregulation of nuclear factor erythroid 2-related factor 2 signaling pathway, Anti Cancer Drugs 31 (1) (2020) 27–34.
[42] H. Chen, Q. Qi, N. Wu, Y. Wang, Q. Feng, R. Jin, L. Jiang, Aspirin promotes RSL3-induced ferroptosis by suppressing mTOR/SREBP-1/SCD1-mediated lipogenesis in PIK3CA-mutatnt colorectal cancer, Redox Biol. 55 (2022), 102426.

[43] W.M. Awara, A.E. El-Sisi, M.E. El-Sayad, A.E. Goda, The potential role of cyclooxygenase-2 inhibitors in the treatment of experimentally-induced mammary tumour: does celecoxib enhance the anti-tumour activity of doxorubicin? Pharmacol. Res. 50 (5) (2004) 487–498.
[44] Y. Xu, Y. Liu, K. Li, D. Yuan, S. Yang, L. Zhou, Y. Zhao, S. Miao, C. Lv, J. Zhao, COX-2/PGE2 pathway inhibits the ferroptosis induced by cerebral ischemia reperfusion, Mol. Neurobiol. 59 (3) (2022) 1619–1631.
[45] S.S. Karuppagounder, L. Alin, Y. Chen, D. Brand, M.W. Bourassa, K. Dietrich, C. M. Wilkinson, C.A. Nadeau, A. Kumar, S. Perry, J.T. Pinto, V. Darley-Usmar, S. Sanchez, G.L. Milne, D. Pratico, T.R. Holman, S.T. Carmichael, G. Coppola, F. Colbourne, R.R. Ratan, N-acetylcysteine targets 5 lipoxygenase-derived, toxic lipids and can synergize with prostaglandin E2 to inhibit ferroptosis and improve outcomes following hemorrhagic stroke in mice, Ann. Neurol. 84 (6) (2018) 854–872.
[46] J. Lu, Y. Zhao, M. Liu, J. Lu, S. Guan, Toward improved human health: Nrf2 plays a critical role in regulating ferroptosis, Food Funct. 12 (20) (2021) 9583–9606.
[47] H. Dong, Z. Qiang, D. Chai, J. Peng, Y. Xia, R. Hu, H. Jiang, Nrf2 inhibits ferroptosis and protects against acute lung injury due to intestinal ischemia reperfusion via regulating SLC7A11 and HO-1, Aging (Albany NY) 12 (13) (2020) 12943–12959.
[48] P. Guan, Y. Liang, N. Wang, Fasudil alleviates pressure overload-induced heart failure by activating Nrf2-mediated antioxidant responses, J. Cell. Biochem. 119 (8) (2018) 6452–6460.
[49] A. Mata, S. Cadenas, The antioxidant transcription factor Nrf2 in cardiac ischemia-reperfusion injury, Int. J. Mol. Sci. 22 (21) (2021), 11939.
[50] L. Zhao, Y. Qi, L. Xu, X. Tao, X. Han, L. Yin, J. Peng, MicroRNA-140-5p aggravates doxorubicin-induced cardiotoxicity by promoting myocardial oxidative stress via targeting Nrf2 and Sirt2, Redox Biol. 15 (2018) 284–296.
[51] C. Tonelli, I.I.C. Chio, D.A. Tuveson, Transcriptional regulation by Nrf2, Antioxidants Redox Signal. 29 (17) (2018) 1727–1745.
[52] A. Kobayashi, M.I. Kang, Y. Watai, K.I. Tong, T. Shibata, K. Uchida, M. Yamamoto, Oxidative and electrophilic stresses activate Nrf2 through inhibition of ubiquitination activity of Keap1, Mol. Cell Biol. 26 (1) (2006) 221–229.
[53] H.C. Huang, T. Nguyen, C.B. Pickett, Regulation of the antioxidant response element by protein kinase C-mediated phosphorylation of NF-E2-related factor 2, Proc. Natl. Acad. Sci. U. S. A. 97 (23) (2000) 12475–12480.
[54] H.C. Huang, T. Nguyen, C.B. Pickett, Phosphorylation of Nrf2 at Ser-40 by protein kinase C regulates antioxidant response element-mediated transcription, J. Biol. Chem. 277 (45) (2002) 42769–42774.
[55] S. Fittipaldi, N. Mercatelli, I. Dimauro, M.J. Jackson, M.P. Paronetto, D. Caporossi, Alpha B-crystallin induction in skeletal muscle cells under redox imbalance is mediated by a JNK-dependent regulatory mechanism, Free Radic. Biol. Med. 86 (2015) 331–342.
[56] C.Y. Tsai, C.C. Wang, T.Y. Lai, H.N. Tsu, C.H. Wang, H.Y. Liang, W.W. Kuo, Antioxidant effects of diallyl trisulfide on high glucose-induced apoptosis are mediated by the PI3K/Akt-dependent activation of Nrf2 in cardiomyocytes, Int. J. Cardiol. 168 (2) (2013) 1286–1297.
[57] M. Buelna-Chontal, J.G. Guevara-Chavez, A. Silva-Palacios, O.N. Medina-Campos, J. Pedraza-Chaverri, C. Zazueta, Nrf2-regulated antioxidant response is activated by protein kinase C in postconditioned rat hearts, Free Radic. Biol. Med. 74 (2014) 145–156.
[58] J.L. Diaz-Ruiz, A. Macias-Lopez, F. Alcala-Vargas, J.G. Guevara-Chavez, A. Mejia-Uribe, A. Silva-Palacios, A. Zuniga-Munoz, C. Zazueta, M. Buelna-Chontal, Redox signaling in ischemic postconditioning protection involves PKCepsilon and Erk1/2 pathways and converges indirectly in Nrf2 activation, Cell. Signal. 64 (2019), 109417.